

Proxy Prompt: Endowing SAM & SAM 2 with Auto-Interactive-Prompt for Medical Segmentation

Anonymous confName submission

Paper ID paperID

arXiv:2502.03501v1 [eess.IV] 5 Feb 2025

WANG XINYI

The Hong Kong Polytechnic University
haylee-xinyi.wang@connect.polyu.hk

KANG HONGYU

The Hong Kong Polytechnic University
hong-yu.kang@connect.polyu.hk

WEI PEISHAN

The Hong Kong Polytechnic University
peishan.wei@polyu.edu.hk

SHUAI LI

The Hong Kong Polytechnic University
sshuai.li@connect.polyu.hk

YU SUN

The Hong Kong Polytechnic University
sunxinbrier@foxmail.com

SAI KIT LAM¹

The Hong Kong Polytechnic University
saikit.lam@polyu.edu.hk

YONGPING ZHENG¹

The Hong Kong Polytechnic University
yongping.zheng@polyu.edu.hk

Abstract

In this paper, we aim to address the unmet demand for automated prompting and enhanced human-model interactions of SAM and SAM2 for the sake of promoting their widespread clinical adoption. Specifically, we propose Proxy Prompt (PP), auto-generated by leveraging non-target data with a pre-annotated mask. We devise a novel 3-step context-selection strategy for adaptively selecting the most representative contextual information from non-target data via vision mamba and selective maps, empowering the guiding capability of non-target image-mask pairs for segmentation on target image/video data. To reinforce human-model interactions in PP, we further propose a contextual colorization module via a dual-reverse cross-attention to enhance interactions between target features and contextual-embedding with amplifying distinctive features of user-defined object(s). Via extensive eval-

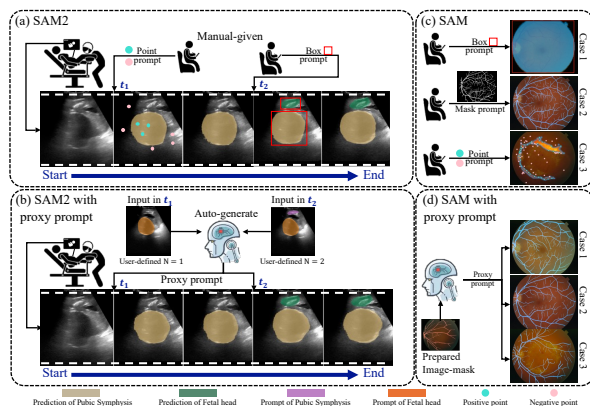


Figure 1. Illustration of comparison without/with PP in (a-b) SAM 2 using real-time ultrasound frames of 1 subject; and (c-d) SAM using a fundus retina dataset of 3 subjects.

uations, our method achieves state-of-the-art performance on four public datasets and yields comparable results with fully-trained models, even when trained with only 16 image masks.

1. Introduction

Under the paradigm shifts in Large-scale Vision Models (LVMs), Segment Anything Model (SAM) [13] and SAM 2 [19] have been introduced as generalized foundation models for segmenting and tracking any objects on image and video data, respectively. These models provide a certain degree of interactive segmentation capacity as users can segment any target object(s) according to their needs by using a single model in-one-go. Such capabilities are achieved by leveraging the concept of prompts [24], such as points, boxes, or masks, waiving the traditional demand for massive manual annotations. Instead, users are only required to input prompts directly on target images or video frames.

Notwithstanding, widespread clinical adoptions of these

¹Sai Kit LAM and Yong-ping ZHENG are also affiliated with the Department of Biomedical Engineering and the Research Institute for Smart Ageing. Both authors are corresponding authors.

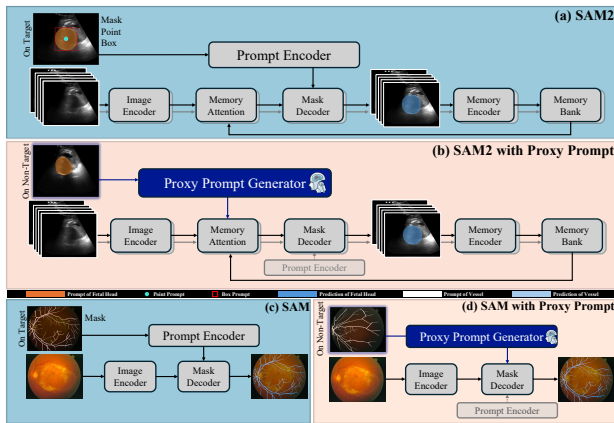


Figure 2. Schematic differences of traditional prompt encoder and our proposed PPG in SAM 2 (a-b) and SAM (c-d).

LVMs have been substantially impeded by the soaring medical demands for “automated prompting” and “high-level human-model interactions” when it comes to downstream medical tasks, particularly real-time imaging-guided interventions. The current prompting strategies are sub-optimal for two key reasons. First, medical image/video data entails an overwhelmingly huge variations in terms of complexity of the target object(s) to be segmented; segmenting such structures (*e.g.* vessels) using existing prompts can be practically challenging. As illustrated in Fig. 1(c), for instance, manually inputting either box prompt (Case 1) or point prompt (Case 3) generates poor results; while adopting mask prompt (Case 2) performs well, it is highly tedious, exhaustive and knowledge-demanding for precise mask prompt formation. Second, users are required to input prompt for every single target image/video frame, which is a manual trial-and-error process, tedious, and not user-friendly. Clinical burden becomes exceedingly prominent when segmenting intricate structures Fig. 1(c) and/or massive datasets, especially in resource-limited clinics. Therefore, there is a pressing demand for automated prompt generation to accommodate various clinical needs.

Apart from this, the existing SAM-based models [21, 28, 30] are inadequate to support the growing demand of high-level human-model interaction to accommodate multifarious clinical goals and high disparity in preferences of clinical users. These models segment target object(s) via training on specific single/multiple object(s). Yet, they do not adapt well to changes in the user’s preferences. For instance, in fundus imaging, optic disc/cup weights more for glaucoma detection [22], while vessels are prioritized for assessing retinal vascular occlusion [20]. Even though these objects may appear within the same image, switching segmentation task from the optic disc/cup to vessels necessitates retraining the model. In real-world clinics where tasks are greatly diverse, creating separate models for individual tasks is practically challenging and computational

demanding. Therefore, it is imperative to reinforce human-model interaction capacity by allowing users to flexibly adjust prompts for satisfying various clinical demands without the need for model retraining. For example, in intrapartum ultrasound as illuminated in Fig. 1(a), these properties would provide high flexibility for users to segment fetal head (FH) alone or FH&pubic symphysis (PS) at any time points $\{t_1, t_2\}$ to achieve measurement of fetal head rotation or fetal position [4].

Confronted with these, we propose a novel Proxy Prompt (PP), which can be automatically generated from a “non-target” data (*i.e.*, image/video frame of subjects other than the one under examination, such as from retrospective datasets) with a pre-annotated mask. This PP strategy is distinct from the existing prompting methods where prompting can only be made on “target” data, in a manual manner. As illustrated in Fig. 1(d), only one annotated image is required in using PP, tremendously streamlining workflow by waiving the prerequisite of providing separated prompts for every image/frame. Moreover, clinicians can freely switch segmentation tasks by adjusting the support-pair input anytime during examination without model retraining nor adopting different models, as shown in Fig. 1(b). Working in tandem with PP, we innovated a Proxy Prompt Generator (PPG) to reform SAM and SAM 2 for image and video data, respectively. Compared to SAM and SAM 2 in Fig. 2 (a&c), we employed high dimensional embedding from the PPG as prompts in Fig. 2 (b&d).

The core design of PPG lies in the novel Contextual Selective Module (CSM) and Contextual Colorization Module (CCM), which are dedicatedly configured for automated prompting and high-level human-model interactions. First, CSM is introduced to enable adaptive selection of the most representative contextual information from “non-target” data for the “target” data, achieving cross-data guidance. Besides, CSM contains Vision Mamba, Bridge Unit, and Selective Map, implementing a 3-step selection process: (i) input-driven, (ii) object-guided, and (iii) target image/frame relevance selection to support both cross-video tasks and cross-image prompting.

Second, CCM is devised to reinforce human-model interaction, enabling the model to interpret diverse user needs as indicated by different masks (*e.g.* single/multiple objects). This aim is achieved by leveraging dual-reverse cross-attention to enhance the representation of contextual embedding. Finally, the PP, effectively capturing specific object features, is generated. Such PPG-based strategy presents a simple yet efficient architecture to enhance clinical-friendliness of SAM and SAM 2, even in few-shot settings. Furthermore, with all original parameters frozen, our design can function as a flexible, plug-and-play module and can continuously adapt to the ever-evolving LVMs beyond SAM and SAM 2.

We conducted extensive experiments across several popular image and video datasets, validating the superior performance and stability of our proposed approach. Our main contributions are outlined below:

1. We propose a novel PP to enhance user-friendliness and precision of SAM and SAM 2 by equipping them with the capacity of automated prompting and high-level human-model interaction.

2. We devise CSM for adaptive selection of the most representative contextual information from “non-target” data to guide segmentation on “target” data, enabling effective cross-image/video prompting, waiving the need to execute prompting for every single target data, and minimizing experience-/expertise-derived variability in prompt quality.

3. We configurate CCM for enhancing the expressiveness of contextual embeddings to interpret and accommodate diverse clinical demands and preference of end users, thereby reinforcing model-human interactions.

4. Extensive experiments show that our model achieves state-of-the-art (SOTA) performance and is comparable to traditional segmentation models trained on full data volumes, even with only 16 image-mask pairs for SAM and SAM 2 training. Moreover, our strategy is of high potential to adapt to the iterative evolution of LVMs for medical tasks in the future.

2. Related Work

2.1. Adapting SAM to Medical Image Segmentation

Given the domain gap between natural and medical image datasets, various works [16, 21, 27, 30] have studied the application of SAM to medical image segmentation. Medical SAM (MedSAM) [16] fine-tunes the decoder of SAM using 1,570,263 medical image-mask pairs with bounding box prompts to adapt to medical tasks. Medical SAM Adapter (Med-SA) [27] efficiently fine-tunes SAM using adapter with point and box prompts. SAM Medical (SAMed) model [30] efficiently fine-tunes the image encoder of SAM using another technique—low-rank-based (LoRA) strategy [9]. AutoSAM [21] utilizes the gradients provided by a frozen SAM to train a new encoder, thus automatically extracts prompts from the image itself to achieve automatic segmentation. However, these SAM-based works on medical data can be roughly categorized into two types: one inherits the prompt design of SAM but without the automatic capability (MedSAM and Med-SA); the other can automatically segment objects but sacrifices the human-model interaction (SAMed and AutoSAM).

2.2. SAM without Manual Given Prompt

In addition to SAMed and AutoSAM, many other works also focus on enhancing the automatic prompting capability of SAM to improve user-friendliness. Self-prompting

SAM [28] fine-tune a self-prompt unit to first provide coarse segmentations, from which they extract point/box prompts for SAM to obtain the final results. Personalization approach for SAM (PerSAM) [31] identify the most similar point between the reference and test image as the prompt for SAM. Evidential prompt generation method (EviPrompt) [29] and ProtoSAM [1] both adapt the idea in PerSAM into medical image domain. EviPrompt fits the point prompts according to image similarity, while ProtoSAM utilizes reference image/mask pair to obtain a coarse segmentation of target image, then extracts point or box as prompts required by SAM. However, these methods are still limited in simulating prompts such as points or boxes, which restricts their capability in the vessel-like branching structures due to the ambiguous instruction [16]. In contrast, our PP emphasizes the high-level embeddings as prompts, thereby guiding the model with deeper-level information to precisely segment such intricate objects.

2.3. Vision Backbone Based on Mamba

To extract contextual information for guiding model segmentation, the recently designed Mamba can serve as a potential choice for building vision backbone. Based on the state space model (SSM) [5], Mamba [6] boosts the development of SSM from the key aspects of “structure”. In terms of structure, it breaks the input-invariant feature of the conventional SSM layer and constructs an input-dependent SSM layer, enabling it to focus on the effective information in the input. Various studies [12, 15, 17, 32, 33] have migrated Mamba to the vision domain. Facial Expression Recognition-YOLO-Mamba (FER-YOLO-Mamba) [15] combines Mamba with attention to construct a dual-branch structure for facial expression detection. Vision Mamba-Denoising Diffusion Probabilistic Model (VM-DDPM) [12] introduces Mamba in the medical image synthesis domain, utilizing an SSM-CNN hybrid structure within the diffusion model. Vision Mamba (Vim) solely relies on the SSM to construct a vision backbone, selectively capturing key information in the input-dependent manner, making it highly suitable for handling high-resolution inputs [33], which is common in medical tasks.

3. Method

Our proposed PPG, compatible with SAM and SAM 2, is illustrated in Fig. 3. Utilizing support image-mask pairs, this network not only enables auto-segmentation on target images or videos but also builds human-model interaction based on user-provided mask. For a target \mathbf{X} , we define a support set $S = \{s_i\}_{i=1}^N$ to assist in the segmentation of N objects within the target \mathbf{X} . Each s_i comprises K image and mask pairs denoted as $s_i = \{(\mathbf{I}^j, \mathbf{M}_i^j)\}_{j=1}^K$, where each image $\mathbf{I}^j \in \mathbb{R}^{3 \times H^0 \times W^0}$ and the correspond-

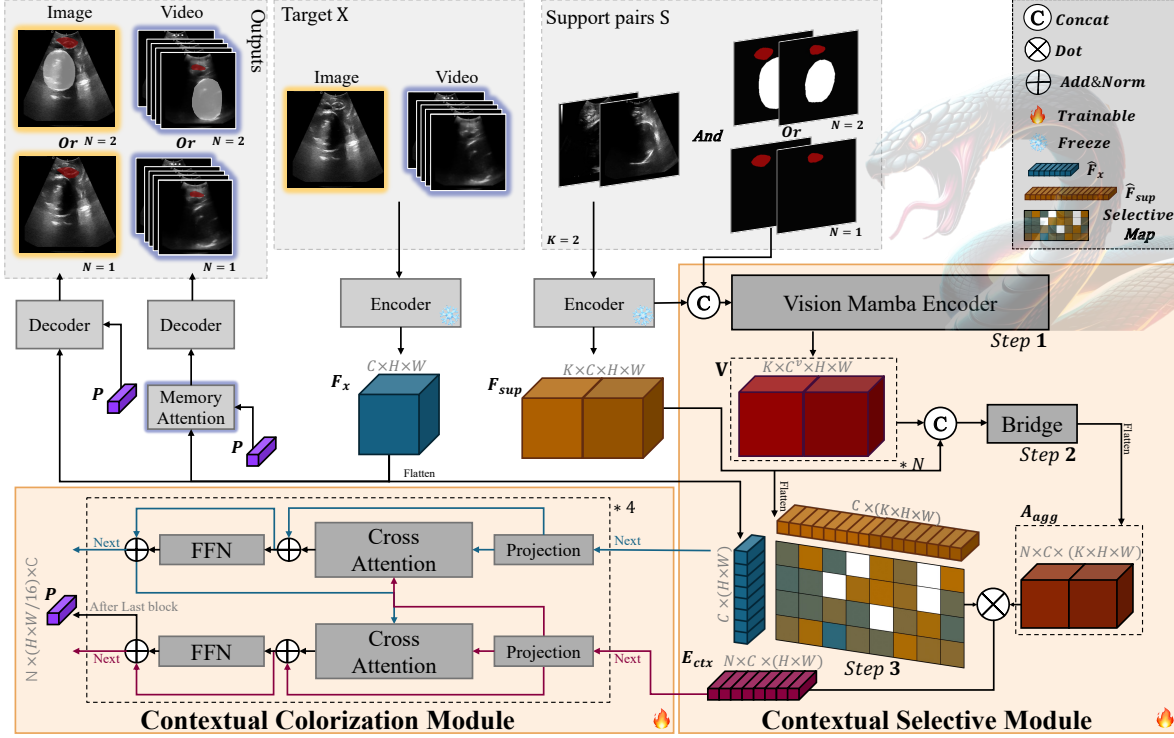


Figure 3. Designed Proxy Prompt Generator for both SAM 2 and SAM. Our key designed focus on the Contextual Selective Module and the Contextual Colorization Module. The Encoder and Decoder refer to the original structures, which are frozen.

ing mask $M_i^j \in \mathbb{R}^{H^0 \times W^0}$. First, the target X and support images $\{I^j\}_{j=1}^K$ are processed by a shared image encoder, with LoRA [9] applied to adapt with medical tasks, resulting in $F_x \in \mathbb{R}^{C \times H \times W}$ and $F_{sup} \in \mathbb{R}^{K \times C \times H \times W}$. In parallel, our Contextual Selective Module (CSM) processes the support pairs through a three-layer selection mechanism to identify the most valuable contextual information for target segmentation, thereby enabling cross-frame prompting (Sec. 3.1). Secondly, the contextual information E_{ctx} is refined within the Contextual Colorization Module (CCM), “coloring” target features with user specifications via dual-reverse cross-attention to achieve human-model interaction (Sec. 3.2). Finally, this refined high-level embedding—enriched with user-defined information and object-specific target feature—serves as a high-dimensional prompt for SAM or SAM 2 (Sec. 3.3). In summary, our method offers three main characteristics: cross-frame guidance, human-model interaction, and high-dimensional prompting via CSM and CCM. In the following sections, we detail each module step-by-step.

3.1. Contextual Selective Module

We leverage Vision Mamba [33]’s selective input capabilities, establish communication between different objects, and design a filtering mechanism to refine the contextual embedding. As illustrated in Fig. 3, support pairs $\{s_i\}_{i=1}^N$ are initially processed by the Vision Mamba encoder to

extract feature V with input-adaptive parameters, marking the first selective step. Secondly, within the designed Bridge Unit, we enable inter-object communication across the concatenated features, thereby selecting information from object-level to form A_{agg} . Thirdly, features (F_x) and (F_{sup}) are used to compute a Selective map. Each row in this map representing a given patch from a support image will positively influence a specific patch in X . This selective map subsequently filters the aggregated information A_{agg} to derive the most valuable information as the contextual embedding E_{ctx} . The following sections will detail each component of this pipeline.

First Selection Step: Vision Mamba. We use the encoder of Vision Mamba (Vim) [33] as the contextual encoder, due to its natural alignment with our needs through its input-dependent selection mechanism. This mechanism enables parameters (i.e., \bar{A} , \bar{B} and C) influencing interactions within the image to adapt as functions of the input, allowing features to be extracted based on the input itself. Specifically, Vim first flattens the input 2-D image into patches and form the token sequence x , which is progressively transformed into the output token sequence y according to the following formula, ultimately being encoded by us into the feature matrix.

$$h_t = \bar{A}h_{t-1} + \bar{B}x_t \quad (1)$$

$$y_t = Ch_t \quad (2)$$

where t represents the timestep and h denotes the latent state. The parameters $\bar{\mathbf{A}}$, $\bar{\mathbf{B}}$ and \mathbf{C} are generated depending on the input x , rather than being input-invariant, thus allowing us to selectively encode the input image as our first step in the selection strategy. For more details, refer to [33].

Given the support set $S = \{s_i\}_{i=1}^N$, we fix a value K such that each $s_i = \{(\mathbf{I}^j, \mathbf{M}_i^j)\}_{j=1}^K$ provides K support pairs $(\mathbf{I}^j, \mathbf{M}_i^j)$. For the j -th pair $\{(\mathbf{I}^j, \mathbf{M}_i^j)\}_{i=1}^N$ among the N support subset s_i , each masks \mathbf{M}_i^j correspond to one same image \mathbf{I}^j . As a result, \mathbf{I}^j is concatenated with \mathbf{M}_i^j and fed into the contextual encoder, resulting in N feature matrices $\mathbf{V} \in \mathbb{R}^{K \times C^v \times H \times W}$, where C^v indicates the channel of \mathbf{V} . The process of extracting the feature matrix \mathbf{V} can be briefly represented by the following equation:

$$\mathbf{V} = \text{Vision Mamba Encoder}(\text{concat}(\mathbf{I}^j, \mathbf{M}_i^j)) \quad (3)$$

Second Selection Step: Bridge Unit. Subsequently, in the Bridge Unit, we initially duplicate N times the obtained feature \mathbf{F}_{sup} and concat with \mathbf{V} of each object along the channel dimension to further aggregate the features. Most importantly, we employ convolutional block attention module (CBAM) [26] along the concatenated channel dimension to facilitate implicit inter-target communication, allowing the model to select key features across multiple objects, thereby enhancing cross-target contextual understanding. Additionally, two ResBlocks [7] are used to prevent further feature dimension expansion. After the final block, the feature is flattened to form \mathbf{A}_{agg} . This process is summarized as follows:

$$\mathbf{F}_{\text{cat}} = \text{concat}(\mathbf{F}_{\text{sup}}, \mathbf{V}) \quad (4)$$

$$\mathbf{A}_{\text{agg}} = \text{ResBlock}_2(\text{CBAM}(\text{ResBlock}_1(\mathbf{F}_{\text{cat}}))) \quad (5)$$

where $\mathbf{F}_{\text{cat}} \in \mathbb{R}^{K \times (N \times (C^v + C)) \times H \times W}$ and $\mathbf{A}_{\text{agg}} \in \mathbb{R}^{N \times C \times (K \times H \times W)}$ represents the aggregated features of the support set.

Third Selection Step: Selective Map. In order to select the key information for the target features, we compute the selective map based on \mathbf{F}_x and \mathbf{F}_{sup} . First, \mathbf{F}_x and \mathbf{F}_{sup} are flattened into $\hat{\mathbf{F}}_x \in \mathbb{R}^{C \times (H \times W)}$ and $\hat{\mathbf{F}}_{\text{sup}} \in \mathbb{R}^{C \times (K \times H \times W)}$, respectively. Then, map is calculated through matrix multiplication, and the calculation is performed using the following equation:

$$\text{Selective} = \frac{2 \cdot (\hat{\mathbf{F}}_{\text{sup}}^T \cdot \hat{\mathbf{F}}_x) - \hat{\mathbf{F}}_{\text{sup}}^2}{\sqrt{C}} \quad (6)$$

where C is the channel dimension of $\hat{\mathbf{F}}_{\text{sup}}$ and $\text{Selective} \in \mathbb{R}^{(K \times H \times W) \times (H \times W)}$. Afterward, the computed Selective is normalized using the softmax to ensure that the contribution values conform to a probability distribution. The resultant information matrix can be represented as follows:

$$\mathbf{E}_{\text{ctx}} = \mathbf{A}_{\text{agg}} \cdot \text{Softmax}(\text{Selective}) \quad (7)$$

where \mathbf{E}_{ctx} serves as the contextual (ctx) embedding of the key information from the support set, and $\mathbf{E}_{\text{ctx}} \in \mathbb{R}^{N \times C \times (H \times W)}$.

3.2. Contextual Colorization Module

The CCM is proposed to interpret user intent from the contextual embedding derived from the support set, enabling human-model interaction. Conceptually, this process is similar to ‘‘colorizing’’ the target image based on the support mask. Unlike the CSM, which focuses on selecting contextually representative information tailored to the target image, this module emphasizes dynamically refining target features on the ground of the contextual embedding via cross-attention, thereby facilitating a deeper understanding of the user’s segmentation intent. Before entering the module, $\hat{\mathbf{F}}_x$ is duplicated N times to align its dimensions with \mathbf{E}_{ctx} .

The CCM consists of four identical blocks, one of which is detailed in Fig. 3. In each block, $\hat{\mathbf{F}}_x$ and \mathbf{E}_{ctx} are each passed through a learnable projection layer to reduce their dimensions to $\hat{\mathbf{F}}_x \in \mathbb{R}^{N \times C \times (H \times W/2)}$ and $\mathbf{E}_{\text{ctx}} \in \mathbb{R}^{N \times C \times (H \times W/2)}$, respectively. Subsequently, \mathbf{E}_{ctx} is integrated into the target image features to guide the model in identifying specific regions expected to be ‘‘colored’’. This integration occurs by adding cross-attention-processed information back into $\hat{\mathbf{F}}_x$, followed by a feed-forward layer (FFN) [23] for contextual reasoning, yielding $\hat{\mathbf{F}}_{x,\text{next}}$, which then serves as the **next** target feature input for the next block. This process is represented as follows:

$$\hat{\mathbf{F}}'_x = \text{Add\&Norm}(\text{Cross Attention}(\hat{\mathbf{F}}_x, \mathbf{E}_{\text{ctx}})) \quad (8)$$

$$\hat{\mathbf{F}}_{x,\text{next}} = \text{Add\&Norm}(\text{FFN}(\hat{\mathbf{F}}'_x)) \quad (9)$$

Subsequently, \mathbf{E}_{ctx} reads from the updated target image features $\hat{\mathbf{F}}_{x,\text{next}}$ through a reversed cross-attention layer to pinpoint features essential for matching object information in the contextual embedding. In the followed FFN, the context embedding, equipped with object-specific feature representation, undergoes further enhancement to strengthen its segmentation guidance capability. The resulting $\mathbf{E}_{\text{ctx},\text{next}}$ then serves as the **next** context embedding for the next block. This process can be expressed as follows:

$$\mathbf{E}'_{\text{ctx}} = \text{Add\&Norm}(\text{Cross Attention}(\mathbf{E}_{\text{ctx}}, \hat{\mathbf{F}}_{x,\text{next}})) \quad (10)$$

$$\mathbf{E}_{\text{ctx},\text{next}} = \text{Add\&Norm}(\text{FFN}(\mathbf{E}'_{\text{ctx}})) \quad (11)$$

After passing through the final block, the iteratively refined context embedding fully comprehends the user-defined segmentation intent from the support set, as well as the corresponding image features derived from the target image. This enhanced context embedding subsequently serves as N prompts \mathbf{P} for the SAM or SAM 2 model, where $\mathbf{P} \in \mathbb{R}^{N \times (H \times W/16) \times C}$.

3.3. Loss Function

For SAM, the image features \mathbf{F}_x extracted from the target image \mathbf{X} is fed into the Decoder with the prompt \mathbf{P} to generate the final output, represented by the following equation:

$$\text{Output} = \text{Decoder}(\mathbf{F}_x, \mathbf{P}) \quad (12)$$

where $\text{Output} \in \mathbb{R}^{N \times H^0 \times W^0}$. For SAM 2, our approach directly inputs the high-dimensional vector \mathbf{P} into memory attention as prompt embeddings, thus \mathbf{P} also can be considered as memory extracted across video frames. For loss settings, we simply follow the design of SAM [13] to supervise the mask prediction with a Dice loss [18], using the following formula:

$$\mathcal{L} = 1 - \frac{2 \sum_{i=1}^D p_i g_i}{\sum_{i=1}^D p_i + \sum_{i=1}^D g_i} \quad (13)$$

where p_i and g_i represent the probability of pixel i in the predicted mask and the label of pixel i in the ground truth mask, respectively. The number of pixels involved in the computation of the Dice loss is denoted by D .

4. Experiment

4.1. Datasets

We conducted extensive experiments on four widely used publicly available datasets, including REFUGE2 [3], STARE [8], FH-PS-AOP(FPA) [11], and JNU-IFM [14]. Among these, STARE [8] contains only one single target, while the other datasets contain multiple segmentation targets. REFUGE2 [3], STARE [8] and FPA [11] are image datasets evaluated in the image segmentation task, whereas JNU-IFM [14] is a video dataset assessed in the video task. Further introduction to the datasets can be found in the supplementary materials.

4.2. Implementation Details

The ‘‘ViT-B’’ SAM model was used and initialized with pre-trained weights. Due to the limited training data, we freeze the pre-trained parameters of SAM to avoid overfitting. We applied LoRA [9] on original encoder and decoder for efficient fine-tuning on medical datasets. The patch size and embedding dimension of ViM [33] encoder were set to 16 and 192, respectively. Model optimization was performed using the Stochastic Gradient Descent (SGD) optimizer, with a momentum of 0.9, a learning rate of 0.01, and a weight decay of 0.0005. Data augmentation was applied to enrich the training process under limited data conditions. This included random variations in image brightness, rotation angles, and shear angles. Specifically, subtle adjustments were made to image saturation, brightness, and contrast within a range of 0.1 to simulate different settings

and image gains. The maximum random rotation angle was set to 15 degrees, and the shear angle was limited to 10 degrees. For each training iteration, a consistent augmentation was applied to all images and masks in the support set.

4.3. Comparison with SOTA on Video Dataset

In this present work, we conducted a comprehensive comparison on the JNU-IFM dataset across four models: MedSAM 2, SAM 2-box, SAM 2-point, and Ours. MedSAM 2 and Ours utilize the image-mask pair to achieve automatic prompting in real-time scenarios, experiments settings can be found in the supplementary materials. Consequently, the simplest prompt in real-time is provided by Ours and MedSAM 2, followed by SAM-point with only one click, and finally SAM-box. Although mask prompts have superior performance based on the most complex information, they are practically overwhelming by a single operator to implement in real-time scenarios, thus serves as our ‘‘Upper’’.

We conducted five experiments on the same test set across the four models to evaluate their performance and stability. We randomly excluded five videos from five patients and paired the first frame’s image and mask as five candidate support pairs. In each experiment, we altered different support pair as prompt to assess stability.

The quantitative comparison results are shown in Fig. 4. From the averaged performance across five experiments, it can be observed that our method improves the dice score by 17.5% compared to MedSAM 2, which uses a similarly simple prompt strategy. Even when compared to SAM 2-box, which employs the most demanding prompt strategy, our method still achieves a 2.3% improvement and is comparable to the ‘‘Upper’’. In terms of stability, MedSAM 2 is significantly affected by variations in the support pairs across the five trials. This results in a maximum dice score fluctuation of 29.1% for MedSAM 2, whereas our method maintains a far smaller fluctuation of only 1.0%.

The qualitative comparison results are shown in Fig. 5. Support pair 1 and 2 were chosen to demonstrate the stability of MedSAM 2 and our model under different prompts. Due to the blurred FH boundary in this case, both SAM 2-box and Ours (as well as the ‘‘Upper’’) exhibited slight over-segment in FH segmentation. However, while SAM 2-box over-segmented the FH region to the left in $Frame_t$, our method constrains this expansion. Although MedSAM 2 showed a notable drop in PS segmentation performance with support pair 1, our method maintained consistent results.

4.4. Comparison with SOTA on Image Dataset

We extensively evaluated diverse comparison methods, including train-free foundation models, models efficiently fine-tuned on the specific-dataset, and traditional segmentation models. Experiment settings of prompts are in the sup-

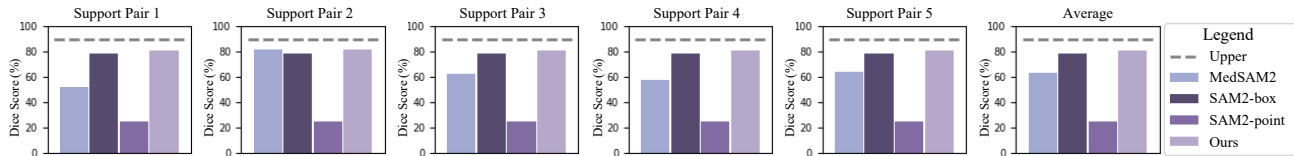


Figure 4. Comparison on the video dataset using five different support pairs, showing the average results for two objects. Results show that our method achieves SOTA performance over existing models and demonstrates stability with a maximum fluctuation of only 1.0%.

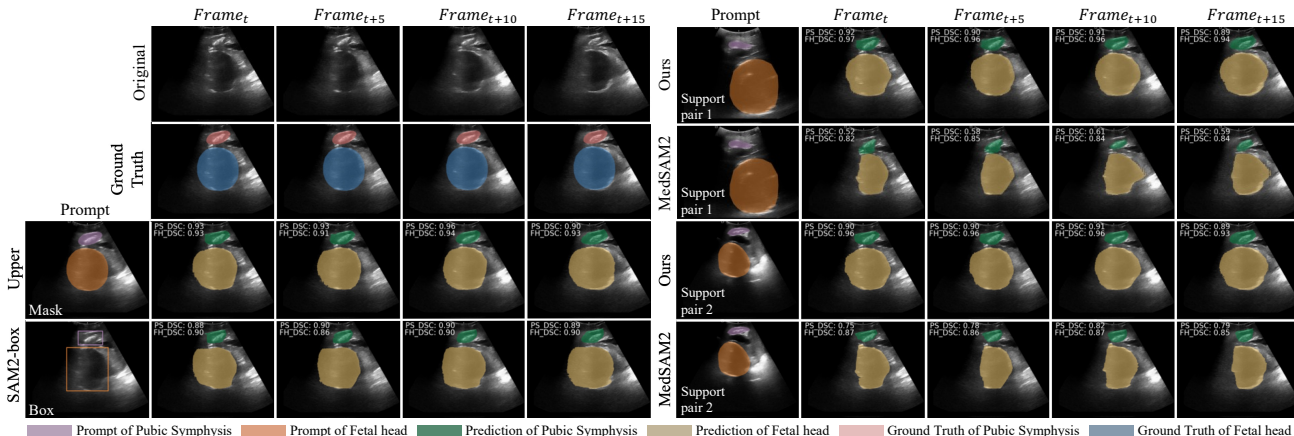


Figure 5. Comparison on one representative video. The top left corner of each subplot displays the Dice scores for the segmentation of the public symphysis (PS_DSC) and fetal head (FH_DSC).

plementary materials. For train-free models such as SAM and MedSAM, we tested their performance with different prompt. Since MedSAM have been pre-trained on a large medical dataset, we evaluated its performance on both the pre-trained FPA dataset and the unseen REFUGE2 dataset. For models requiring training, including Med-SA, SAMed, AutoSAM, and ours, we trained each model on the same 16 images until full convergence to evaluate their performance in few-shot settings. For traditional segmentation models, we used dataset-specific SOTA methods, including BEAL [25] for REFUGE2, nnUnet [10] for STARE, and Segnet [2] for FPA. The results of the three models, as claimed in their papers, were obtained under full data training settings and thus were treated as the “Upper”.

The quantitative comparison results are presented in Tab. 1. MedSAM and AutoSAM showed strong performance in both train-free and few-shot settings, probably due to pre-training on large medical datasets or object-specific training. However, MedSAM’s performance dropped significantly on unseen datasets and struggled with intricate structure such as vessel in the STARE dataset. AutoSAM, on the other hand, underperformed on ultrasound datasets, possibly due to the challenges such as ultrasound imaging-associated speckle noise. Furthermore, AutoSAM requires training five models for five objects, whereas our method only requires training two models for two modalities with human-model interaction. This reduction in retraining enhances practicality in real-world clinics, where tasks are more diverse. Our method achieved SOTA performance

under limited conditions, even comparable with traditional SOTAs trained on the full dataset.

The qualitative comparison results are presented in Fig. 6. For the REFUGE2 dataset, SAMed and AutoSAM performed relatively well, nevertheless both showed issues with missing regions in the boundaries for certain objects. On the vascular dataset STARE, MedSAM with box prompt exhibited ambiguity, confusing the objects to be segmented. For PS in the FPA dataset, most models tended to over-segment, with SAM-point, SAM-box, Med-SA, and AutoSAM extending the PS segmentation beyond the object’s lower right boundary, while SAM-everything and SAMed less segment in the lower left edge. For FH, most models tended to over-segment, while SAM-box and SAMed exhibited less segmentation at the upper left edge. This may be caused by blurring of the object boundary due to presence of speckle noise in the ultrasound dataset. Across all datasets, our method consistently produced superior and stable results.

4.5. Ablation Studies

For each dataset, 16 samples were excluded to ensure a consistent test set across all experiments. To evaluate the impact of training set size M , we defined **Train set** = $\{(I_i, M_i)\}_{i=1}^M$ with $M \in \{2, 4, 8, 16\}$, setting the number of support pairs to $M - 1$ during training. For a given M , we conducted repeated experiments by randomly selecting multiple independent and diverse **Support set** = $\{(I_i, M_i)\}_{i=1}^G$ for each inference support

Method	Training times	Color fundus photography			Ultrasound		Average
		REFUGE2-Disc	REFUGE2-Cup	STARE-Vessel	FPA-PS	FPA-FH	
Upper*	5	93.7	83.5	65.5	82.1	91.7	83.3
SAM ^{TF} (1-point)	-	39.1	33.5	16.3	18.2	34.4	28.3
SAM ^{TF} (box)	-	54.2	71.6	20.5	67.0	88.0	60.3
SAM ^{TF} (everything)	-	48.8	40.0	20.5	25.6	35.4	34.1
MedSAM ^{TF} (box)	-	87.2	81.3	20.1	97.1	97.5	74.5
Med-SA (1-point)	3	85.6	83.0	45.4	71.3	81.4	73.3
Med-SA (box)	3	86.8	82.6	37.1	71.8	83.1	72.3
SAMed	3	86.9	84.3	15.8	66.3	<u>87.0</u>	68.1
AutoSAM	5	<u>87.9</u>	<u>84.6</u>	<u>73.8</u>	<u>78.0</u>	79.1	<u>80.7</u>
Ours	2	88.2	85.6	78.9	81.5	88.0	84.4

Table 1. Comparison of our model with SAM-based SOTAs in Dice Score (%), including train-free models (denoted as ^{TF}), efficient fine-tuned models, and models trained on full data (denoted as *Upper**). ‘Training times’ records minimum number of trained models required to segment 5 objects, with dash(-) denoting inapplicability. Gray indicates the data were used in model pre-training. The **best** and second-best results (excluding Upper) are bolded and underlined, respectively, showcasing our SOTA performance among various models under same few-shot settings.

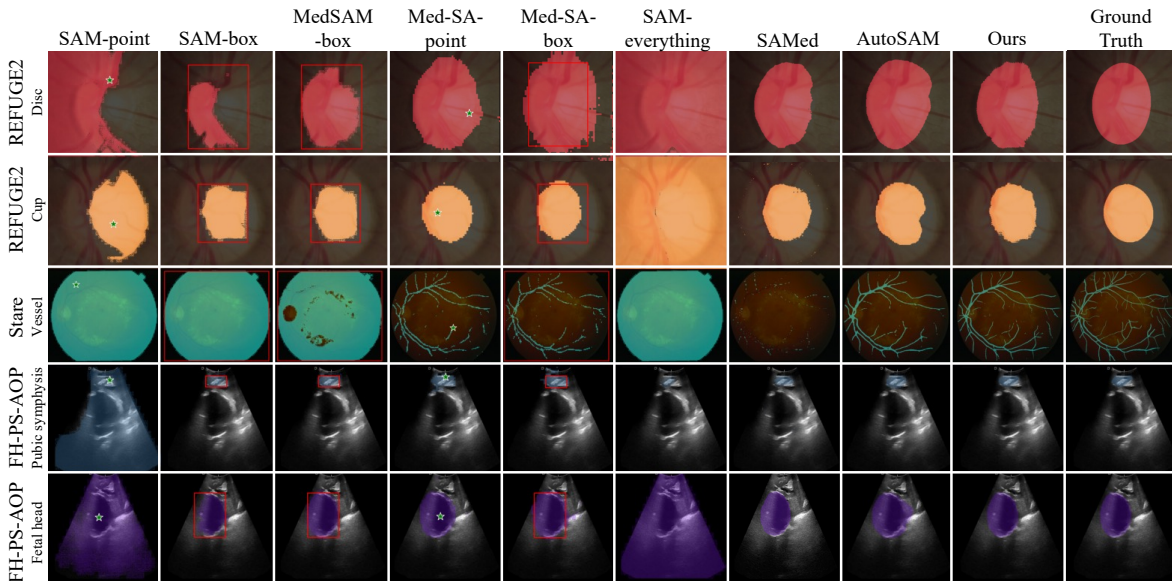


Figure 6. Visualization comparison results of nine models across five objects.

size $G \in \{1, 2, 4, 8\}$. Under different values of M and G , the averaged dice scores across three datasets and five objects are illuminated in Fig. 7.

The figure shows a positive correlation between segmentation quality and M . For each M , the dice score monotonically increases with G until G exceeds $M - 1$, after which a slight decline may occur. Furthermore, the ridge plot reveals that when $G = 1$, the distribution of dice scores is more dispersed due to the highly diverse **Support set**. However, as G increases, the variance in model predictions with various support pairs greatly decreases. For instance, in the top-right plot based on $M = 16$, the results of repeated experiments are more concentrated with sharper shape when $G = 8$ (teal region) compared to $G = 1$ (charcoal purple region), indicating that the model is less affected by the quality of individual support pairs. In sum-

mary, both training dataset size M and inference support size G influence model performance, with M having a notably greater impact. The dice score stabilizes at its highest value when both M and G are maximized, reflecting the optimal performance and stability of our model.

Experiments validating the effectiveness of the two modules are provided in the supplementary materials.

5. Conclusion

We present the PPG, a pluggable framework designed to endow SAM and SAM 2 with auto-prompting and enhanced their interactive capabilities. Our PPG employs a CSM to extract contextual information from non-target data and a CCM to interpret user intentions, enabling it to generate efficient PP that effectively guides the model output to meet user needs. The PPG also can be implanted into other LVMs, continuously integrating cutting-edge foundation

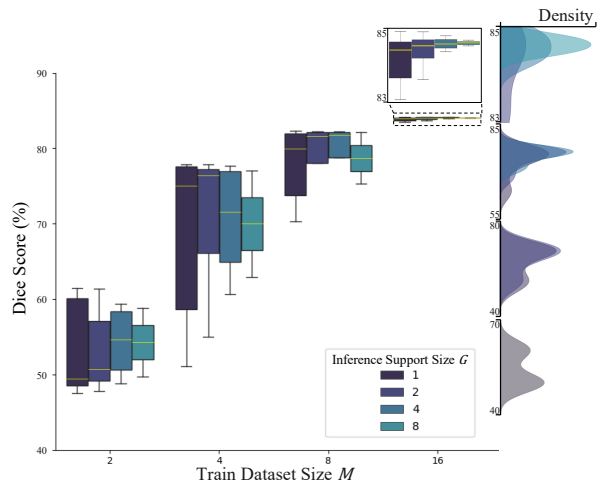


Figure 7. The boxes show performance for each M with varying G , while in the rightmost plots ($G < M - 1$), higher peaks refer to better performance and narrower ranges reflect improved stability. Optimum is achieved when both M and G are maximized.

models to meet the evolving demands in widespread medical applications.

References

- [1] Lev Ayzenberg, Raja Giryes, and Hayit Greenspan. Proto-sam: One-shot medical image segmentation with foundational models. *ArXiv*, abs/2407.07042, 2024. 3
- [2] Vijay Badrinarayanan, Alex Kendall, and Roberto Cipolla. Segnet: A deep convolutional encoder-decoder architecture for image segmentation. *IEEE transactions on pattern analysis and machine intelligence*, 39(12):2481–2495, 2017. 7
- [3] Huihui Fang, Fei Li, Junde Wu, Huazhu Fu, Xu Sun, Jaemin Son, Shuang Yu, Menglu Zhang, Chenglang Yuan, Cheng Bian, et al. Refuge2 challenge: A treasure trove for multi-dimension analysis and evaluation in glaucoma screening. *arXiv preprint arXiv:2202.08994*, 2022. 6
- [4] T Ghi, T Eggebø, C Lees, K Kalache, P Rozenberg, A Youssef, LJ Salomon, and B Tutschek. Isuog practice guidelines: intrapartum ultrasound. *Ultrasound in Obstetrics & Gynecology*, 52(1):128–139, 2018. 2
- [5] Albert Gu. *Modeling Sequences with Structured State Spaces*. Stanford University, 2023. 3
- [6] Albert Gu and Tri Dao. Mamba: Linear-time sequence modeling with selective state spaces. *arXiv preprint arXiv:2312.00752*, 2023. 3
- [7] Kaiming He, Xiangyu Zhang, Shaoqing Ren, and Jian Sun. Deep residual learning for image recognition. In *Proceedings of the IEEE conference on computer vision and pattern recognition*, pages 770–778, 2016. 5
- [8] AD Hoover, Valentina Kouznetsova, and Michael Goldbaum. Locating blood vessels in retinal images by piecewise threshold probing of a matched filter response. *IEEE Transactions on Medical imaging*, 19(3):203–210, 2000. 6
- [9] Edward J Hu, Yelong Shen, Phillip Wallis, Zeyuan Allen-Zhu, Yuanzhi Li, Shean Wang, Lu Wang, and Weizhu Chen. Lora: Low-rank adaptation of large language models. *arXiv preprint arXiv:2106.09685*, 2021. 3, 4, 6
- [10] Fabian Isensee, Paul F Jaeger, Simon AA Kohl, Jens Petersen, and Klaus H Maier-Hein. nnu-net: a self-configuring method for deep learning-based biomedical image segmentation. *Nature methods*, 18(2):203–211, 2021. 7
- [11] Bai Jieyun and Ou ZhanHong. Pubic Symphysis-Fetal Head Segmentation and Angle of Progression, 2023. 6
- [12] Zhihan Ju and Wanting Zhou. Vm-ddpm: Vision mamba diffusion for medical image synthesis. *arXiv preprint arXiv:2405.05667*, 2024. 3
- [13] Alexander Kirillov, Eric Mintun, Nikhila Ravi, Hanzi Mao, Chloe Rolland, Laura Gustafson, Tete Xiao, Spencer Whitehead, Alexander C Berg, Wan-Yen Lo, et al. Segment anything. In *Proceedings of the IEEE/CVF International Conference on Computer Vision*, pages 4015–4026, 2023. 1, 6
- [14] Yaosheng Lu, Mengqiang Zhou, Dengjiang Zhi, Minghong Zhou, Xiaosong Jiang, Ruiyu Qiu, Zhanhong Ou, Huijin Wang, Di Qiu, Mei Zhong, Xiaoxing Lu, Gaowen Chen, and Jieyun Bai. The jnu-ifm dataset for segmenting pubic symphysis-fetal head. *Data in Brief*, 41:107904, 2022. 6
- [15] Hui Ma, Sen Lei, Turgay Celik, and Heng-Chao Li. Fer-yolo-mamba: Facial expression detection and classification based on selective state space. *arXiv preprint arXiv:2405.01828*, 2024. 3
- [16] Jun Ma, Yuting He, Feifei Li, Lin Han, Chenyu You, and Bo Wang. Segment anything in medical images. *Nature Communications*, 15(1):654, 2024. 3
- [17] Jun Ma, Feifei Li, and Bo Wang. U-mamba: Enhancing long-range dependency for biomedical image segmentation. *arXiv preprint arXiv:2401.04722*, 2024. 3
- [18] Fausto Milletari, Nassir Navab, and Seyed-Ahmad Ahmadi. V-net: Fully convolutional neural networks for volumetric medical image segmentation. In *2016 fourth international conference on 3D vision (3DV)*, pages 565–571. Ieee, 2016. 6
- [19] Nikhila Ravi, Valentin Gabeur, Yuan-Ting Hu, Ronghang Hu, Chaitanya Ryali, Tengyu Ma, Haitham Khedr, Roman Rädle, Chloe Rolland, Laura Gustafson, et al. Sam 2: Segment anything in images and videos. *arXiv preprint arXiv:2408.00714*, 2024. 1
- [20] S Sekhar, Waleed Al-Nuaimy, and Asoke K Nandi. Automated localisation of optic disk and fovea in retinal fundus images. In *2008 16th European Signal Processing Conference*, pages 1–5. IEEE, 2008. 2
- [21] Tal Shaharabany, Aviad Dahan, Raja Giryes, and Lior Wolf. Autosam: Adapting sam to medical images by overloading the prompt encoder. *arXiv preprint arXiv:2306.06370*, 2023. 2, 3
- [22] Niharika Thakur and Mamta Juneja. Survey on segmentation and classification approaches of optic cup and optic disc for diagnosis of glaucoma. *Biomedical Signal Processing and Control*, 42:162–189, 2018. 2
- [23] A Vaswani. Attention is all you need. *Advances in Neural Information Processing Systems*, 2017. 5
- [24] Jiaqi Wang, Zhengliang Liu, Lin Zhao, Zihao Wu, Chong Ma, Sigang Yu, Haixing Dai, Qiushi Yang, Yiheng Liu,

- Songyao Zhang, et al. Review of large vision models and visual prompt engineering. *Meta-Radiology*, page 100047, 2023. 1
- [25] Shujun Wang, Lequan Yu, Kang Li, Xin Yang, Chi-Wing Fu, and Pheng-Ann Heng. Boundary and entropy-driven adversarial learning for fundus image segmentation. In *Medical Image Computing and Computer Assisted Intervention—MICCAI 2019: 22nd International Conference, Shenzhen, China, October 13–17, 2019, Proceedings, Part I 22*, pages 102–110. Springer, 2019. 7
- [26] Sanghyun Woo, Jongchan Park, Joon-Young Lee, and In So Kweon. Cbam: Convolutional block attention module. In *Proceedings of the European conference on computer vision (ECCV)*, pages 3–19, 2018. 5
- [27] Junde Wu, Wei Ji, Yuanpei Liu, Huazhu Fu, Min Xu, Yanwu Xu, and Yueming Jin. Medical sam adapter: Adapting segment anything model for medical image segmentation. *arXiv preprint arXiv:2304.12620*, 2023. 3
- [28] Qi Wu, Yuyao Zhang, and Marawan Elbatel. Self-prompting large vision models for few-shot medical image segmentation. In *MICCAI workshop on domain adaptation and representation transfer*, pages 156–167. Springer, 2023. 2, 3
- [29] Yinsong Xu, Jiaqi Tang, Aidong Men, and Qingchao Chen. Eviprompt: A training-free evidential prompt generation method for segment anything model in medical images. *arXiv preprint arXiv:2311.06400*, 2023. 3
- [30] Kaidong Zhang and Dong Liu. Customized segment anything model for medical image segmentation. *arXiv preprint arXiv:2304.13785*, 2023. 2, 3
- [31] Renrui Zhang, Zhengkai Jiang, Ziyu Guo, Shilin Yan, Junting Pan, Xianzheng Ma, Hao Dong, Peng Gao, and Hongsheng Li. Personalize segment anything model with one shot. *arXiv preprint arXiv:2305.03048*, 2023. 3
- [32] Zhuoran Zheng and Jun Zhang. Fd-vision mamba for endoscopic exposure correction. *arXiv preprint arXiv:2402.06378*, 2024. 3
- [33] Lianghai Zhu, Bencheng Liao, Qian Zhang, Xinlong Wang, Wenyu Liu, and Xinggang Wang. Vision mamba: Efficient visual representation learning with bidirectional state space model. *arXiv preprint arXiv:2401.09417*, 2024. 3, 4, 5, 6

Proxy Prompt: Endowing SAM & SAM 2 with Auto-Interactive-Prompt for Medical Segmentation

Supplementary Material

F. Additional Ablation Experiment

We conducted ablation experiments to validate the effectiveness of the Contextual Selective Module (CSM) and Contextual Colorization Module (CCM) modules. To assess the contribution of CCM in interpreting diverse user segmentation intention, we presented results on the FH-PS-AOP (FPA) dataset under two different indications to segment pubic symphysis (PS) and fetal head (FH). All settings were tested on the same test set, excluding data from 16 subjects for support image-mask pairs. To segment the PS structure in the FPA dataset (FPA-PS), we used the excluded original images and PS masks as inputs to the Proxy Prompt Generator (PPG), replacing the mask with the Fetal Head (FH) mask for FH segmentation (FPA-FH).

Table 2. Ablation experiments on different modules of Proxy Prompt Generator on the FH-PS-AOP dataset, with results reported in terms of Dice scores.

CSM	CCM	FPA-PS	FPA-FH	Average
✓	✓	81.5	88.0	84.8
✓	✗	79.4	88.4	83.9
✗	✓	80.3	87.3	83.8
✗	✗	78.3	87.5	82.9

The results in Tab. 2 highlight the contributions of both CSM and CCM to the optimal model performance. When CCM was removed, the segmentation performance for PS structures showed a pronounced decline (2.1% Dice score drop), while FH structures exhibited a slight improvement. This may be attributed to the absence of CCM impairing the PPG’s ability to interpret different user intentions, resulting in markedly divergent segmentation outcomes under varying indications. On the other hand, removing CSM led to an overall degradation in segmentation quality for both FH and PS structures, with the average Dice score decreasing by 1%. When the selective mechanism of CSM was disabled and CCM was simultaneously omitted, model performance fell to the Med-SA baseline. This experiment demonstrates that our model, when enhanced with both modules, achieves optimal and consistent performance across different objects.

G. Prompt Strategy

G.1. Settings for Video Dataset.

Considering the high demand for timely operation in real-time image-guided examinations and interventions for physicians, prompt was only required for the first frame of

the video data.

1. **Box:** Minimum bounding rectangle of the target as a bounding box prompt.
2. **Point:** Center point of the object as a positive point.
3. **Mask:** Target mask of the patient under examination.
4. **Support Image-Mask Pair:** Image of the first frame and the corresponding target mask from “non-target” data (i.e., image/video frame of subjects other than the one under examination, such as from retrospective datasets).

G.2. Settings for Image Dataset.

For the models that require prompts in the comparison experiments on image dataset, the following prompt conditions are provided.

1. **Point:** Since the center point of the disc and vessel mask is not on the target, one random point within the target mask as a positive point prompt.
2. **Box:** Minimum bounding rectangle of the target as a bounding box prompt.
3. **Everything:** Automatically segment multiple targets with everything mode. We select the prediction that the highest overlaps with ground truth to calculate the model’s Dice score.
4. **Others:** The SAMed and AutoSAM models are designed to perform automatic segmentation without manual-given prompt, while we use the support image-mask pair as a prompt.

H. Datasets Introduction

Type of image modalities, segmentation objects, and number of samples for the four included datasets are summarized in the table below. The related references are provided in the main text.

Table 3. Dataset summary.

Dataset	Modality	Segmentation Objects	Samples
REFUGE2	Fundus	Optic disc and optic cup	2000 images
STARE	Fundus	Blood vessels in retinal images	20 images
FPA	Ultrasound	Fetal head and pubic symphysis	4000 images
JNU-IFM	Ultrasound	Fetal head and pubic symphysis	78 videos